



Temperature versus composition phase diagrams and spin glass behavior in low dimensional, mixed magnetic systems
by Gerald Victor Rubenacker

A thesis submitted in partial fulfillment of the requirements for the degree of Doctor of Philosophy in Physics
Montana State University
© Copyright by Gerald Victor Rubenacker (1988)

Abstract:

The temperature versus composition phase diagrams for several low dimensional, mixed magnetic systems have been investigated. The magnetic behavior of the pseudo-one-dimensional mixed systems $[(\text{CH}_3)_3\text{NH}]A(1-x)\text{BxCl}_3 \cdot 2\text{H}_2\text{O}$ where A and B are Co, Ni, and Mn, was investigated as a function of x. The mixture with Co and Ni was found to exhibit spin glass behavior below a characteristic temperature T_g as evidenced by the onset of time dependent thermoremanent magnetization. The phase diagram of temperature versus x showed a very broad and deep spin glass region with unusually thin antiferromagnetic phase regions above it. A tetracritical point near $x = 0.58$ was indicated. Thermoremanent magnetization versus time below T_g was fit to a stretched exponential function plus a constant offset term. Mixtures of Mn with Co and Mn with Ni showed no spin glass behavior above 2 K and had a deep depression in the center of their temperature versus x phase diagrams. The pseudo-two-dimensional mixed systems, $[\text{NH}_3(\text{CH}_2)_n\text{NH}_3]\text{CuCl}_4\text{Br}_{4(1-x)}$ for $n = 5$ and 7 were also investigated. The temperature versus x phase diagrams for these systems also showed evidence of tetracritical points but with mixed phase regions rather than spin glass phases. From an examination of the differences in these systems, criteria for development of mixed phases and spin glass phases were discussed.

TEMPERATURE VERSUS COMPOSITION PHASE DIAGRAMS AND SPIN
GLASS BEHAVIOR IN LOW DIMENSIONAL, MIXED
MAGNETIC SYSTEMS

by

Gerald Victor Rubenacker

A thesis submitted in partial fulfillment
of the requirements for the degree

of

Doctor of Philosophy

in

Physics

MONTANA STATE UNIVERSITY
Bozeman, Montana

May, 1988

D378
R822

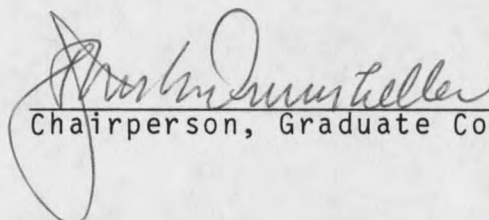
APPROVAL

of a thesis submitted by

Gerald Victor Rubenacker

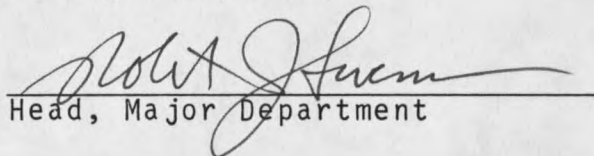
This thesis has been read by each member of the thesis committee and has been found to be satisfactory regarding content, English usage, format, citations, bibliographic style, and consistency, and is ready for submission to the College of Graduate Studies.

19 May 1988
Date


Chairperson, Graduate Committee

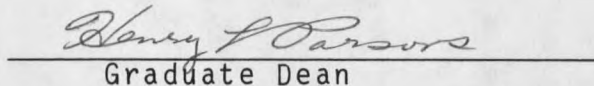
Approved for the Major Department

19 May 1988
Date


Head, Major Department

Approved for the College of Graduate Studies

June 10, 1988
Date


Graduate Dean

STATEMENT OF PERMISSION TO USE

In presenting this thesis in partial fulfillment of the requirements for a doctoral degree at Montana State University, I agree that the Library shall make it available to borrowers under rules of the Library. I further agree that copying of this thesis is allowable only for scholarly purposes, consistent with "fair use" as prescribed in the U. S. Copyright Law. Requests for extensive copying or reproduction of this thesis should be referred to University Microfilms International, 300 North Zeeb Road, Ann Arbor, Michigan 48106, to whom I have granted "the exclusive right to reproduce and distribute copies of the dissertation in and from microfilm and the right to reproduce and distribute by abstract in any format."

Signature *Ronald V. Rasmussen*

Date *19 May 1988*

ACKNOWLEDGMENTS

I would like to extend my special thanks to Professor John Drumheller who has been my advisor on this project. I am also grateful for the help of many others including: Professor Kenneth Emerson, Donald Haines, Stuart Hutton and the M. S. U. Agricultural Analytical Lab.

This work was supported by National Science Foundation grant DMR-8702993.

TABLE OF CONTENTS

INTRODUCTION.	1
Properties of Single Metal MTAC Compounds	3
Previous Work on Mixed MTAC Systems	9
Multicritical Points.	12
Spin Glasses.	16
EXPERIMENTS	19
Sample Preparation and Analysis	19
The Vibrating Sample Magnetometer	22
Measurements on CoNiTAC	26
Magnetization Versus Temperature Measurements.	26
Magnetization Versus Applied Field Measurements.	34
Thermoremanent Magnetization Data.	40
AC Susceptibility of CoNiTAC	41
EPR Measurements on CoNiTAC.	50
MnCoTAC and MnNiTAC Magnetization Measurements.	50
7-DA and 5-DA Magnetic Measurements	54
DISCUSSION.	63
Phase Diagram of CoNiTAC.	63
Model and Fit of the TRM.	69
Spin Glass Dimensionality	74
Phase Diagrams of MnCoTAC and MnNiTAC	75
Phase Diagrams for the 7-DA and 5-DA Compounds.	78
Low Dimensional Mixed Systems: A Comparison	84
CONCLUSIONS	86
REFERENCES CITED.	88

LIST OF TABLES

Table	Page
1. Low temperature phases and critical temperatures for n-DACuX ₄ (F = ferromagnetic ordering and AF = antiferromagnetic ordering).	58
2. Antiferromagnetic transition temperatures T _C and spin glass transition temperatures T _g for various percentages of nickel in CoNiTAC	65
3. Best fits of the parameters t _p , n and M' to Equation (9) for TRM measurements at the given temperatures and nickel concentrations	73
4. Curie and Neel temperatures for MnCoTAC and MnNiTAC mixtures along with their corresponding metal percentages.	78
5. Transition temperatures for various values of x in 5-DACuCl ₄ Br _{4(1-x)}	79
6. Transition temperatures for various values of x in 7-DACuCl ₄ Br _{4(1-x)}	82

LIST OF FIGURES

Figure	Page
1. The cobalt-chloride chain of CoTAC with the a axis perpendicular to the drawing.	5
2. A simplified view of CoTAC looking along the chain direction. Lines represent the orientation of the water molecules. Arrows on the left and right represent two possible spin orientations with respect to the waters	6
3. Thermoremanent magnetization (1 kOe initial field) versus temperature for various waiting times in the 65% nickel sample	13
4. Sketch of a temperature versus x phase diagram with a tetracritical point and a mixed phase region	15
5. Percent nickel in the solutions used to prepare the mixed CoNiTAC samples versus percent nickel in the resultant crystals.	21
6. Magnetization versus temperature at 50 Oe for a powder sample containing 53% nickel. Both zero field cooled and field cooled curves are shown . .	27
7. Magnetization versus temperature at 50 Oe for a single crystal of CoNiTAC containing 30% nickel. Triangles are for the c axis (antiferromagnetic) and circles are for the a axis (ferromagnetic).	29
8. Magnetization versus temperature at 50 Oe for a single crystal of CoNiTAC containing 37% nickel. Open circles are for the c axis (antiferromagnetic) and solid circles are for the a axis (ferromagnetic).	30

Figure	Page
9. Magnetization versus temperature at 50 Oe for a single crystal of CoNiTAC containing 44% nickel. Triangles are for the c axis (antiferromagnetic) and circles are for the a axis (ferromagnetic).	31
10. Magnetization versus temperature at 50 Oe for a single crystal of CoNiTAC containing 58% nickel. Triangles are for the c axis (antiferromagnetic) and solid circles are for the a axis (ferromagnetic).	32
11. Magnetization versus applied field for a single crystal of CoNiTAC containing 37% nickel and oriented along the c or antiferromagnetic axis . .	35
12. Magnetization versus applied field for a single crystal of CoNiTAC containing 58% nickel and oriented along the c or antiferromagnetic axis . .	36
13. Magnetization versus applied field for a single crystal of CoNiTAC containing 37% nickel and oriented along the a or ferromagnetic axis	38
14. Magnetization versus applied field for a single crystal of CoNiTAC containing 58% nickel and oriented along the a or ferromagnetic axis	39
15. Thermoremanent magnetization versus time (50 Oe initial field) for the 34% sample at 2.4, 2.6, 2.8, 3.0 and 3.2 K. The solid lines are fit to a stretched exponential with a constant offset . .	42
16. Thermoremanent magnetization versus time (50 Oe initial field) for the 58% sample. The lines from top to bottom were taken at 2.4, 2.6, 2.8, 3.0 and 3.2 K. The solid line are fit to a stretched exponential with a constant offset . . .	43
17. Thermoremanent magnetization versus time (50 Oe initial field) for the 72% sample. The lines from top to bottom were taken at 2.4, 2.6 and 2.8 K. The solid lines are fit to a stretched exponential with a constant offset	44

Figure	Page
18. Susceptibility versus temperature for a 49% Ni sample of CoNiTAC. Solid line is the real part of the susceptibility along the a axis. Dashed line is the real part of the susceptibility along c axis. Dotted line is the imaginary part of the susceptibility along the a axis. . . .	46
19. Real part of the susceptibility versus temperature for a 60% Ni sample of CoNiTAC along the a axis. Solid line is for a frequency of 160 Hz and dashed line is for 80 Hz.	49
20. Inverse susceptibility versus temperature for MnCoTAC powders. Mixtures containing 20, 30, 40 and 60 percent Co are represented respectively by circles, squares, triangles and double triangles	52
21. Inverse susceptibility versus temperature for MnNiTAC powders. Mixtures containing 10, 20, 30 and 60 percent Ni are represented respectively by circles, squares, triangles and double triangles	53
22. Unit cell of 2-DACuCl ₄ showing the positions of the ions (except hydrogen). Some of the CuCl bonds are included to help show the "puckering" of the layers.	55
23. Powder magnetic susceptibility versus temperature data for n-DACuBr ₄ with n = 5-10. Solid data points are referenced to the left scale and open data points to the right scale. . .	57
24. Susceptibility versus temperature for 5-DACuCl ₄ xBr ₄ (1-x) with x = .12 (circles), .47 (squares), .65 (triangles), .76 (double triangles), and .88 (+'s).	59
25. Susceptibility versus temperature for 7-DACuCl ₄ xBr ₄ (1-x) with x = 0 (circles), .24 (squares), .35 (triangles), .47 (double triangles), .53 (x's), and 1.0 (+'s)	60

Figure	Page
26. Susceptibility versus temperature for a 7-DACuCl ₄ xBr ₄ (1-x) single crystal with x = .24 both parallel (triangles) and perpendicular (circles) to the ferromagnetic planes	62
27. Phase diagram of temperature versus x (mole fraction of nickel) for CoNiTAC showing the paramagnetic, antiferromagnetic, and spin glass regions.	64
28. Phase diagram of temperature versus x (mole fraction of cobalt) for MnCoTAC.	76
29. Phase diagram of temperature versus x (mole fraction of nickel) for MnNiTAC.	77
30. Phase diagram of temperature versus x for 5-DACuCl ₄ xBr ₄ (1-x)	80
31. Phase diagram of temperature versus x for 7-DACuCl ₄ xBr ₄ (1-x)	81

ABSTRACT

The temperature versus composition phase diagrams for several low dimensional, mixed magnetic systems have been investigated. The magnetic behavior of the pseudo-one-dimensional mixed systems $[(\text{CH}_3)_3\text{NH}]A_{(1-x)}B_x\text{Cl}_3 \cdot 2\text{H}_2\text{O}$ where A and B are Co, Ni, and Mn, was investigated as a function of x. The mixture with Co and Ni was found to exhibit spin glass behavior below a characteristic temperature T_g as evidenced by the onset of time dependent thermoremanent magnetization. The phase diagram of temperature versus x showed a very broad and deep spin glass region with unusually thin antiferromagnetic phase regions above it. A tetracritical point near $x = 0.58$ was indicated. Thermoremanent magnetization versus time below T_g was fit to a stretched exponential function plus a constant offset term. Mixtures of Mn with Co and Mn with Ni showed no spin glass behavior above 2 K and had a deep depression in the center of their temperature versus x phase diagrams. The pseudo-two-dimensional mixed systems, $[\text{NH}_3(\text{CH}_2)_n\text{NH}_3]\text{CuCl}_4x\text{Br}_4(1-x)$ for $n = 5$ and 7 were also investigated. The temperature versus x phase diagrams for these systems also showed evidence of tetracritical points but with mixed phase regions rather than spin glass phases. From an examination of the differences in these systems, criteria for development of mixed phases and spin glass phases were discussed.

INTRODUCTION

Systems with randomly mixed magnetic interactions are important to the field of critical phenomena because their temperature versus composition phase diagrams can contain multicritical points. In addition, if there is a frustration in the magnetic interactions, the system may be a type of magnetic material known as a spin glass. The purpose of this work is to investigate the temperature versus composition phase diagram and spin glass behavior for several low dimensional, mixed magnetic systems. Low dimensional systems were chosen for study in order to discuss the effects of dimensionality in mixed magnetic systems.

The mixed systems considered here include three site disordered, pseudo-one dimensional materials with the general formula, $[(\text{CH}_3)_3\text{NH}]\text{MCl}_3 \cdot 2\text{H}_2\text{O}$ in which M represents a mixture of Co-Ni, Mn-Co or Mn-Ni. For example, in the cobalt-nickel mixture M would be replaced by $\text{Co}_{(1-x)}\text{Ni}_x$ in which x is the mole fraction of the metal sites which contain nickel and can have values ranging from zero to one. For ease in reading, trimethylammonium metal trichloride dihydrate or $[(\text{CH}_3)_3\text{NH}]\text{MCl}_3 \cdot 2\text{H}_2\text{O}$ will henceforth be abbreviated as MTAC. For the cobalt and

nickel example above, the abbreviation CoNiTAC would therefore be used. The other mixed systems to be considered are two bond disordered, pseudo-two dimensional systems, $5\text{-DACuCl}_{4x}\text{Br}_{4(1-x)}$ and $7\text{-DACuCl}_{4x}\text{Br}_{4(1-x)}$. Here, 5-DA and 7-DA are abbreviations for pentanediammonium, $\text{NH}_3(\text{CH}_2)_5\text{NH}_3$, and heptanediammonium, $\text{NH}_3(\text{CH}_2)_7\text{NH}_3$, respectively. x is the mole fraction of the total halide that is chloride.

Among these systems, only CoNiTAC was found to behave as a spin glass, and because of the interesting properties of a spin glasses, it was studied in the most detail. Specifically, the results include: single crystal measurements of both dc magnetization and ac susceptibility; thermoremanent magnetization (TRM) measurements and a fit to a theoretical model; and an improved temperature versus x phase diagram. Magnetization measurements for the other systems result in discussion of their temperature versus x phase diagrams. Finally, by comparing these results, the effects of the dimensionality of the interactions can be discussed.

Before discussing the present experiments and their results, a review of previous work on the MTAC systems will be presented. Both pure, single metal compounds and mixed systems will be considered. In addition, some theoretical and experimental background concerning what to

expect from a random mixture phase diagram and from a spin glass will be discussed. No previous work other than our own has been done on the 5-DA and 7-DA copper halides.

Properties of Single Metal MTAC Compounds

In order to discuss the mixed metal systems, it is first necessary to describe the structural and magnetic properties of the pure, single metal compounds. MTAC can be prepared with the divalent metals Co, Ni, Mn, Cu and Fe. The trimethylammonium metal chlorides formed with the above five metals are all isostructural with only small differences in bond lengths and bond angles. As such they make good candidates for mixed magnetic systems since changes in magnetic properties can be associated with the change in the properties of the metal and related only very weakly with changes in the crystal structure. The structure of CoTAC will be described in detail. The other members of this series of compounds can be considered structurally identical to CoTAC with the minor distance and angle corrections mentioned above.

The structure of CoTAC was first solved by Losee et al.¹ In CoTAC the cobalt ions are octahedrally coordinated by two water molecules and four chloride ions with the waters being trans to each other. Two chlorides on each edge are shared with adjacent cobalt octahedra to

form bibridged chains of cobalt octahedra with the stoichiometry $\text{Co}(\text{H}_2\text{O})_2\text{Cl}_2$. A portion of this chain looking along the a axis of the crystal is illustrated in Figure 1. The water molecules hydrogen bond with the remaining chloride ions to form weakly bound planes of cobalt chains. The three dimensional structure is formed by stacking these planes with the trimethylammonium cations spaced between them. The planes are staggered such that cobalt chains in one plane lie between the chains of the next nearest neighbor plane. A simplified structure of CoTAC, looking along the chain or b axis direction, is shown in Figure 2. The short lines indicate the orientation of the H_2O ligands. They are tilted approximately 10 degrees away from the c axis, however the angle in the diagram has been exaggerated in order to emphasize the inequivalence of adjacent planes. Notice that the water ligands are tilted away from the c axis but alternate directions in each successive plane. The structure itself then introduces an alternating anisotropy in the cobalt sites.

Magnetically each cobalt is coupled along the chains through two Co-Cl-Co bonds. This is the strongest exchange path with $J_b/k = 15.4 \text{ K}$. (b denotes the crystallographic b direction and also the chain direction.) This interaction is ferromagnetic, as is the

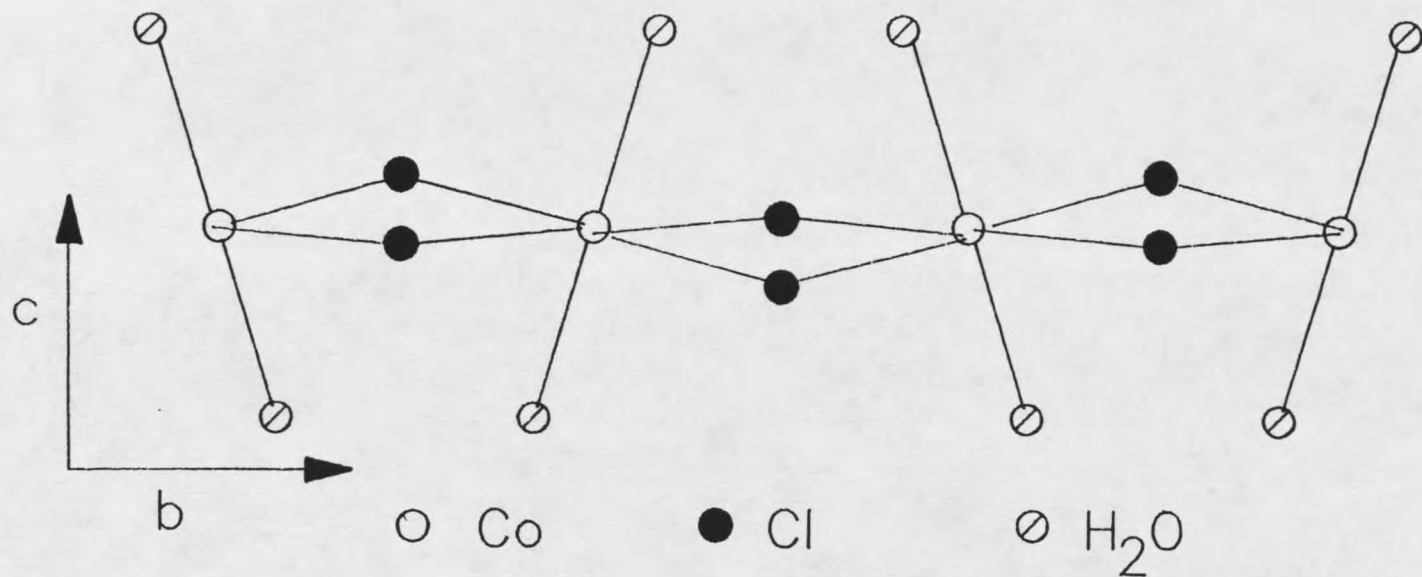


Figure 1. The cobalt-chloride chain of CoTAC with the a axis perpendicular to the drawing.

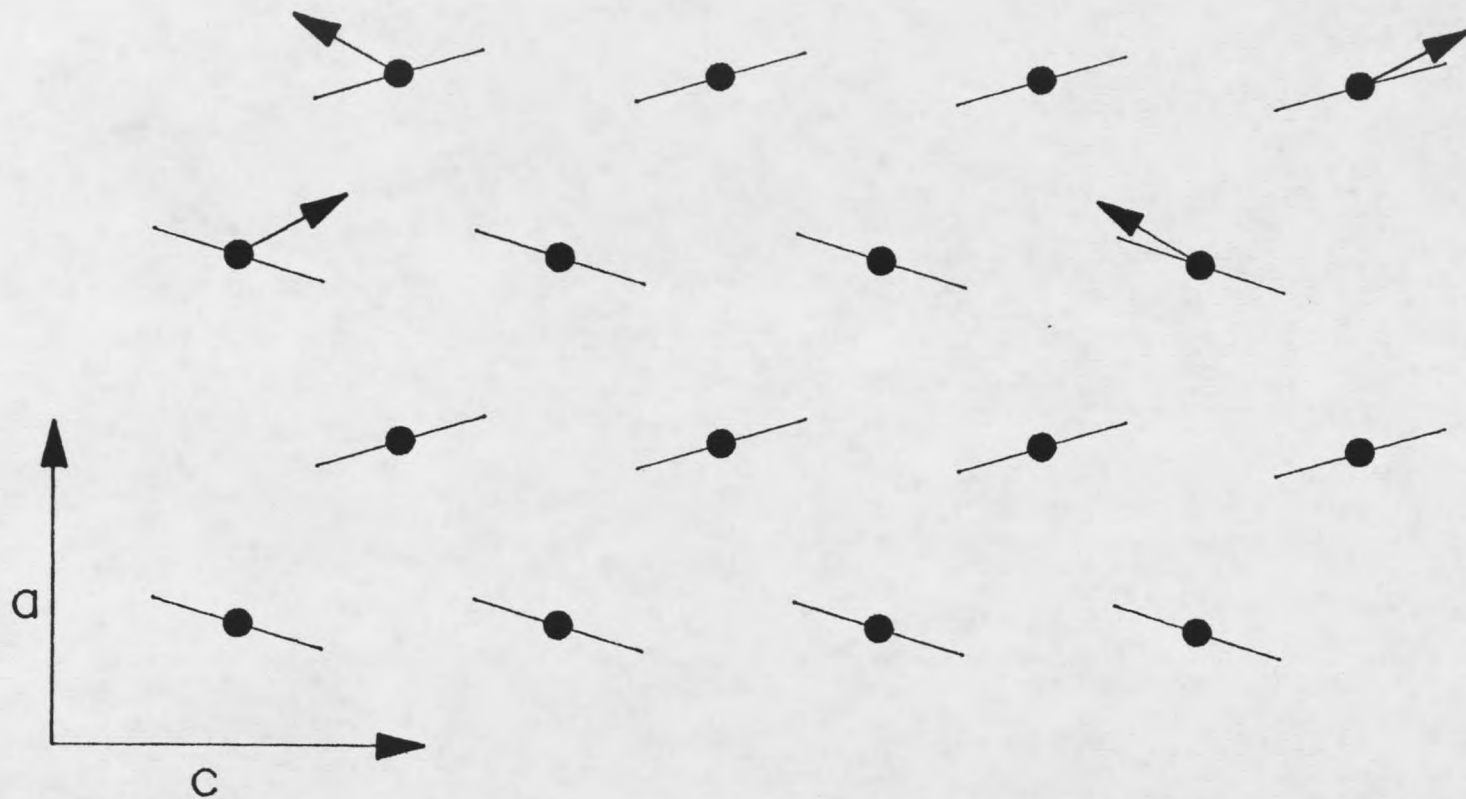


Figure 2. A simplified view of CoTAC looking along the chain direction. Lines represent the orientation of the water molecules. Arrows on the left and right represent two possible spin orientations with respect to the waters.

next strongest coupling in the c axis direction. Since this exchange is through hydrogen bonds with the H₂O ligands, the coupling is much smaller; $J_c/k = 0.1$ K. There is virtually no direct exchange path in the third direction and $J_a/k = -.01$ K is smaller still. This exchange is negative, therefore the overall 3-dimensional ordering is antiferromagnetic. The critical temperature is $T_c = 4.2$ K. The antiferromagnetic or easy axis is along the c direction. The a axis shows weak ferromagnetic behavior indicating that the spins are canted away from the c axis in the a direction. There are two ways in which the spins may be canted with respect to the symmetry of the cobalt sites. They may orient either near the water axis or near the chloride plane as shown respectively on the right and left of Figure 2. The b axis susceptibility is very small indicating that the spins are confined to the ac plane. The susceptibility data was fit to the one dimensional, $S = 1/2$, Ising model for the c and a-axes.^{2,3} The c-axis (easy axis) susceptibility is given as

$$\chi = (Ng^2\mu_B^2/4kT)\exp(2J/kT) \quad (1)$$

and the b-axis or perpendicular susceptibility is given as

$$\chi = (Ng^2\mu_B^2/8J)[\tanh(J/kT)\operatorname{sech}^2(J/kT)]. \quad (2)$$

The standard Ising model, however, could not fit the a-axis susceptibility because of the ferromagnetic canting

in this direction. Instead the expression

$$\chi = Ng^2 u_B^2 (T - T_0) / [4k(T^2 - T_c^2)] \quad (3)$$

for a weak ferromagnet was used.⁴ NMR studies by Spence and Botterman⁵ predict the canting angle to be about 10 degrees from the c direction. They also show a transition at about 60 Oe from an antiferromagnetic to paramagnetic state along the c axis, making this compound a metamagnet. Further ac susceptibility measurements by Groenendijk⁶ and van Duyneveldt^{6,7} confirm the metamagnetic behavior and refine the value of the zero field canting angle to be 22 degrees. The deuterated form of CoTAC was also investigated by Groenendijk et al.⁸ in order to determine the effect on the J_a exchange constant which operates through the hydrogen bonds. However, only a 6% change in J_a was found in this case.

NiTAC is nearly identical structurally to CoTAC as determined by O'Brien et al.⁹ The reported magnetic parameters are also similar with $T_c = 3.7$ K, $J_b/k = 14$ K, $J_c/k = 0.07$ K and $J_a/k = -0.006$ K as reported by Hoogerbeets et al.¹⁰ The spins are again confined to the ac plane with a canting angle of 21 degree from the c direction. Further EPR studies by Hoogerbeets et al.¹¹ confirm the c axis to be the easy axis and b to be the hard axis.

The structure of MnTAC was determined by Caputo et al.¹² and by Depmeier and Klaska¹³ and is also isomorphic to the cobalt and nickel analogs. In contrast to these, however, it has antiferromagnetic coupling along the chains with a Neel temperature of $T_n = 4.1$ K as determined by Simizu et al.¹⁴ The phase diagram for this compound near the bicritical point has been described by Megy et al.¹⁵

The structure of CuTAC was determined by Losee et al.¹⁶ and is similar to CoTAC except that the bridges are assymetrical and CuTAC's crystallographic space group is different. Stirrat et al.¹⁷ found a very weak coupling along the chains with $J/k = 0.85$ K and $T_c = 0.165$ as refined by Algra et al.¹⁸ Ritter et al.¹⁹ have determined the isotropic symmetric, dipolar, anisotropic symmetric and antisymmetric exchange parameters from epr measurements.

FeTAC was investigated by Landee et al.²⁰ with $T_c = 3.28$ K. The spins are Ising-like and lie along the chain axis. The one dimensional ordering is ferromagnetic with an overall three dimensional antiferromagnetic ordering.

Previous Work on Mixed MTAC Systems

Some work on mixed MTAC systems has already been published. Schouten et al.²¹ reported heat capacity

measurements on CoCuTAC. Since the transition temperature of CuTAC is so low, 0.157 K, copper is expected to resemble a diamagnetic impurity and lower the transition temperature of CoTAC as the concentration is increased. It in fact does this but not with the slope that might be expected. This system is best described as a bond impurity system in which three values of the coupling constant, J , are used. The best fit is to $J_{IH} = J_{HH}$ and $J_{II} = 0.02J_{HH}$. Using Schouten's nomenclature J_{HH} , J_{II} and J_{IH} refer respectively to coupling between two nearest neighbor cobalt atoms, two copper atoms and one cobalt and one copper atom. The subscript I refers to the Ising character of cobalt and H refers to the Heisenberg character of copper. The value of J_{IH} disagrees with the usual approximation $J_{IH} = (J_{II}J_{HH})^{1/2}$, and a much closer fit is found by letting $J_{IH} = J_{HH}$.

Some magnetic resonance work on MnCoTAC has also been done by Matsubara et al.²² and by Phaff et al.²³ They find a limiting of the spin diffusion rate as more manganese is added to the crystal. This indicates a decreased coupling between manganese and cobalt, or using the nomenclature introduced in the previous paragraph, J_{IH} is much less than J_{HH} or J_{II} in this system. This is not a surprising result since the cobalt and manganese easy axes are not in the same direction.

Susceptibility and remanence studies have been done on MnCoTAC for small manganese concentrations by Cheikhrouhou et al.²⁴ They find spin glass behavior in this system for very low manganese concentrations. For 2.9% Mn, $T_g = 3.6$ K and for 9.3% Mn, $T_g = 1.76$ K.

Magnetization measurements on powder samples of CoNiTAC have been done by Raffaele.²⁵ Susceptibility as a function of temperature was found for CoNiTAC with various nickel and cobalt metal percentages. Graphs of $1/X$ versus T give straight lines at high temperatures which when extrapolated intersect the temperature axis at the Curie temperature, T_c . For all mixtures the value of T_c was between 4.5 K and 4.1 K with a slight lowering as the nickel percentage was increased.

Two types of experiments were performed to determine the field dependence of the magnetization. The first method was to cool the sample from above T_c in a field of 2000 Oe, then reduce the field to 13 Oe and take measurements as the temperature was increased. For contrast, measurements were then taken in 13 Oe as the temperature was decreased from above T_c . A more standard field cooled and zero field cooled set of curves were also obtained. In this case the sample was cooled in zero field ($H < 4$ Oe), the field was then set to 50 Oe and after waiting 3 minutes measurements were taken as the

temperature was raised. This results in the ZFC or zero field cooled curve. The FC or field cooled curve was obtained by lowering the temperature from above T_c in an applied field of 50 Oe and taking measurements. The susceptibilities separate below a temperature, T_g for the field cooled versus zero field cooled curves.

By doing thermoremanent magnetization studies at various temperatures T_g was also determined by the temperature at which there is no longer a TRM. A graph of the TRM versus temperature for various waiting times is shown in Figure 3 for a 65% Ni sample.²⁶

Using these values of T_c and T_g a preliminary magnetic phase diagram of temperature versus mole fraction of nickel was constructed. The phase diagram has been refined in this work by correcting the values of the nickel concentrations and by adding more data points to the diagram.

Multicritical Points

A tricritical point occurs in a magnetic phase diagram where two second order phase transition lines meet with a line of first order phase transitions. The classic example of this is seen in the field versus temperature phase diagram of an antiferromagnet. The tricritical point occurs where the second order paramagnetic to

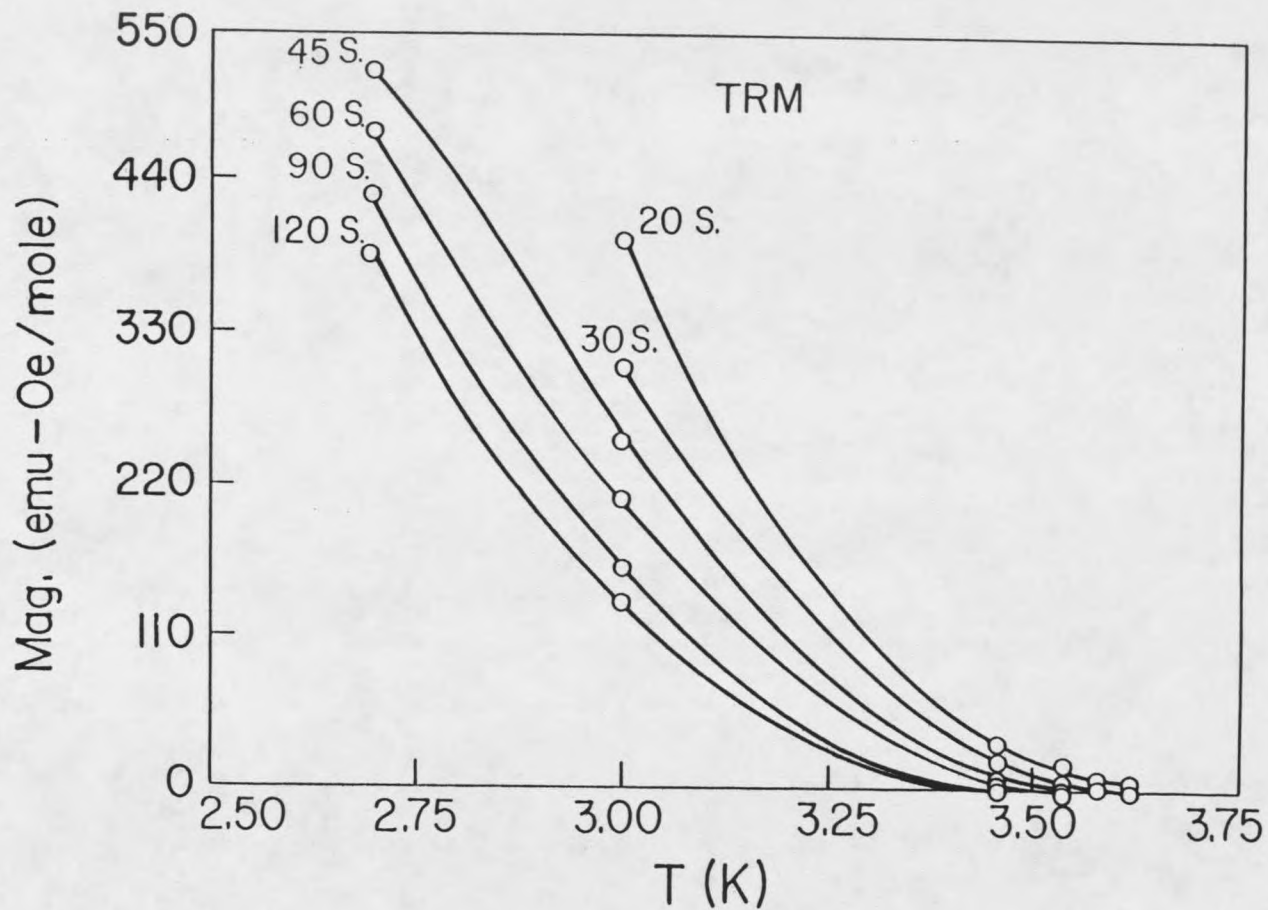


Figure 3. Thermoremanent magnetization (1 kOe initial field) versus temperature for various waiting times in the 65% nickel sample.

antiferromagnetic and paramagnetic to spin flop lines meet with the first order antiferromagnetic to spin flop line. A tetracritical point occurs where four lines of second order phase transitions meet or equivalently where two lines of second order phase transitions cross. Multicritical points not only occur in temperature versus field phase diagrams but also in temperature versus composition phase diagrams where there are two competing interactions. How critical lines come together at a tetracritical point is of interest theoretically,²⁷⁻³⁰ and it is predicted that they should meet tangentially and not at an angle.

An example of this can be found in the temperature versus composition phase diagram of two antiferromagnets with different easy axes. A representation of this type of phase diagram is shown schematically in Figure 4 and would be appropriate for a system such as $\text{Fe}_{(1-x)}\text{Co}_x\text{Cl}_2 \cdot 2\text{H}_2\text{O}$.³¹ The pure iron and cobalt compounds each have transitions from a paramagnetic to antiferromagnetic phase as temperature is lowered, but the easy axes are in different directions due to differences in anisotropy between iron and cobalt. A new phase lies between these two antiferromagnetic phases and represents a spin alignment which is in an intermediate direction. This mixed phase region is not characterized by a single

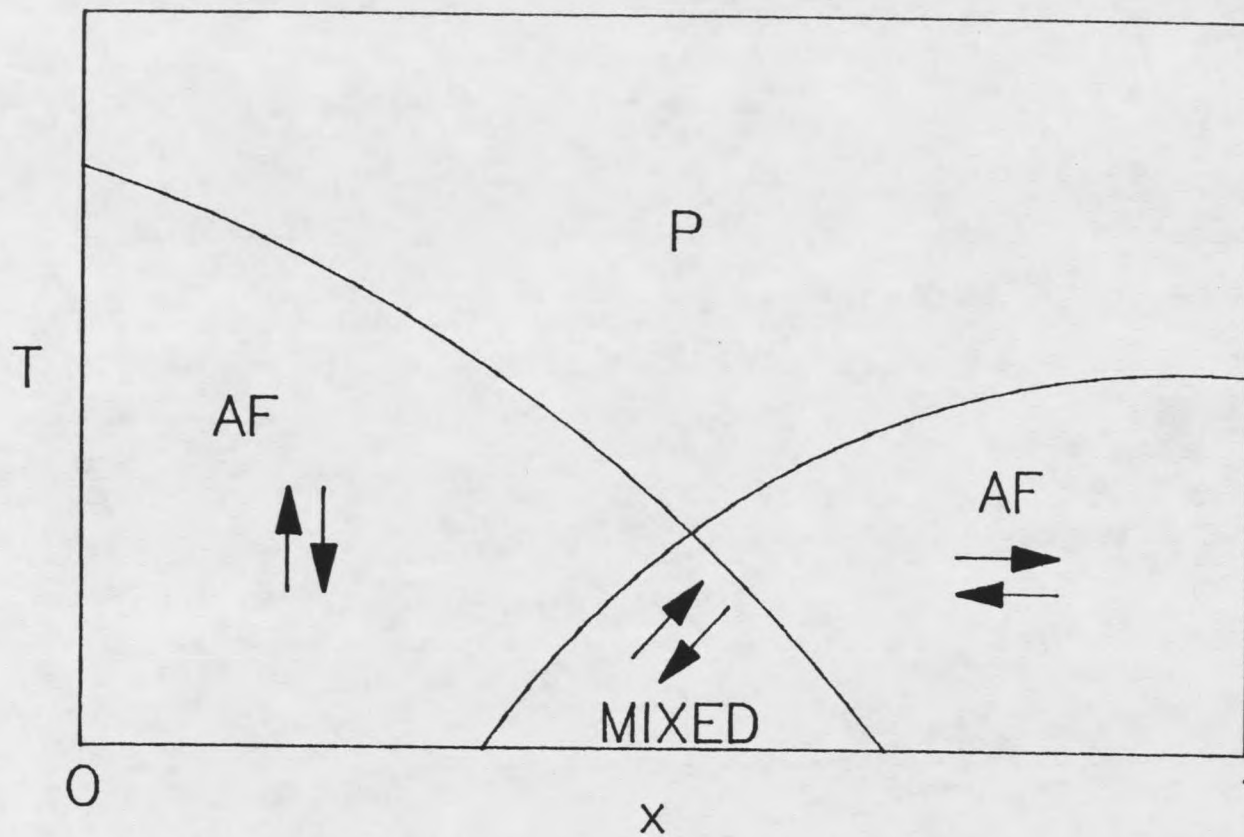


Figure 4. Sketch of a temperature versus x phase diagram with a tetracritical point and a mixed phase region.

intermediate direction but by a gradual change in the spin orientation. For a constant low temperature but with increasing x , the spin direction remains constant until the antiferromagnetic to mixed phase boundary is reached. The spin direction then gradually shifts until the high x orientation is reached and the second mixed to antiferromagnetic phase boundary is crossed. The tetracritical point occurs where the four lines in the diagram meet. If the competing anisotropy between the two magnetic sites were made larger, the mixed phase would become narrower until the critical lines came together to form a single first order line with a tricritical point. The 5-DA and 7-DACuCl_{4x}Br_{4(1-x)} systems will be discussed in terms of a tetracritical system as illustrated in Figure 4, however there is not only competing anisotropy but also a competing antiferromagnetic to ferromagnetic competition. In contrast, the large anisotropies in CoNiTAC suggest a very narrow or nonexistent mixed phase region.

Spin Glasses

Extensive reviews on the spin glass phenomena have been published by Anderson,³² Mydosh³³, Fisher^{34,35} and Binder and Young.³⁶ The word "glass" as used here refers to an amorphous or random system in which there is a

"viscosity" or time dependent change in some thermodynamic variable. For an ordinary glass this corresponds to a shape (volume) change with time when a pressure change is introduced; for a ferroelectric glass this is a dielectric susceptibility change with time for a change in the applied electric field; and for a spin glass this is a change in magnetization with time for a change in the applied magnetic field.

Two properties are recognized as necessary but not always sufficient conditions to produce a spin glass. First, there must be randomness in the arrangement of at least two types of spins, and second, there must be frustration. Frustration results when two competing interactions try to drive the spins toward different lowest energy states. For spin glasses there are three common types of frustration: magnetic versus non-magnetic lattice sites, ferromagnetic versus antiferromagnetic exchange and competing anisotropies.

Given the minimal conditions to obtain a spin glass, one must then ask what properties must such a system possess to be called a spin glass. Again there are three recognized properties:³⁶ first, magnetic moments must be frozen in below a temperature, T_g , such that a cusp results in ac susceptibility versus temperature measurements at T_g ; second, there must be magnetic

relaxation on a macroscopic time scale below T_g when there are changes in the magnetic field; third there is a lack of long-range magnetic order. This third condition, however, can be relaxed as in the CoNiTAC system presented in this work in which the spin glass state occurs along with a ferromagnetic state. The dc magnetization and ac susceptibility data for CoNiTAC will be considered in relation to the first two criteria.

EXPERIMENTS

Sample Preparation and Analysis

Many of the CoNiTAC crystals and powders and the n-DA powders were prepared for these experiments by Professor Kenneth Emerson of the MSU Chemistry Department. (n-DA is used here as an abbreviation for the whole series of diammonium copper tetrachlorides.) The rest of the samples were prepared in this laboratory. In general the metal halides and the ammonium halides were dissolved in water such that the ratio of metal to amine was 1:1. The metal ratio in the MTAC compounds and the halide ratio in the n-DA compounds were adjusted to obtain the various mixed compounds. One drop of concentrated HCl was added to each MTAC solution since an acidic solution was found to increase crystal size in NiTAC.⁸ The solutions were allowed to evaporate undisturbed and the resulting precipitates were removed by filtration.

The MTAC crystals formed do not contain the same metal percentages as the solutions from which they were prepared. The metal percentages in MnCoTAC and MnNiTAC samples were obtained from graphs of manganese as percent of total metal in solution versus mole fraction manganese

in the crystals as determined by Lindbeck.³⁷ The metal percentages in CoNiTAC were determined by atomic absorption analyses for cobalt and nickel. Analyses were commissioned from the MSU Agricultural Analytical Lab and from Galbraith Laboratories. Using these results, a graph of nickel as percent of total metal in the preparative solutions versus mole fraction nickel in the crystals for CoNiTAC was obtained and is presented in Figure 5. Scatter in the data points in Figure 5 is not due to errors in the percent nickel in the solutions or the metal analyses of the crystals and so must be attributed to random variations in how the crystallization takes place. The slope of the curve in Figure 5 is not as steep as the curve determined by Lindbeck³⁷ and again may be a result of the method of preparation.

Small crystals of CoNiTAC weighing up to 0.3 mg were obtained from the initial preparations. Because of the large, low temperature magnetic moment of CoNiTAC, this small size was sufficient for magnetic measurements. The crystals are uniform in appearance and the three crystallographic axes are easily identified visually. The crystals are needle-like with the long axis being the b-axis. They are also dichroic and are purple to brown when looked at along the c-axis and green along the a-axis.

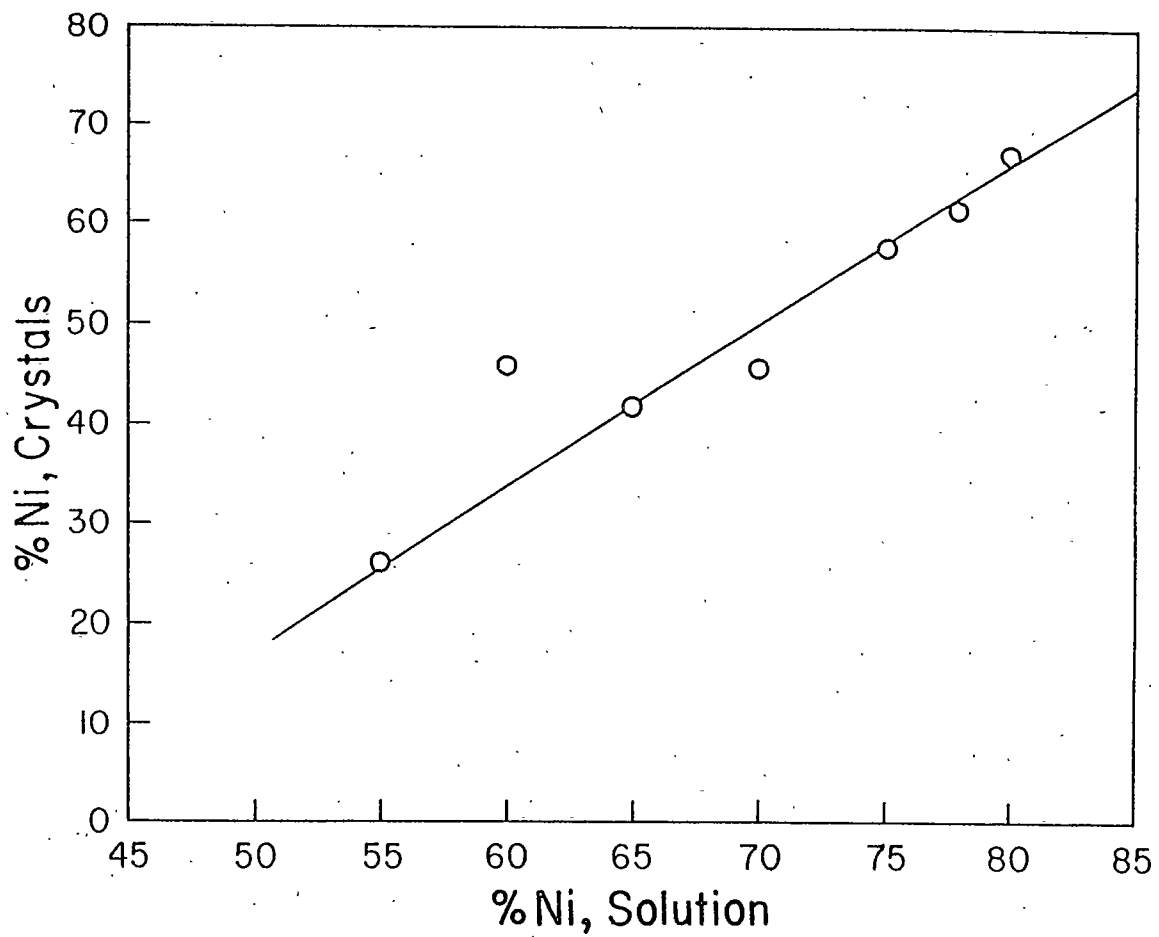


Figure 5. Percent nickel in the solutions used to prepare the mixed CoNiTAC samples versus percent nickel in the resultant crystals.

A constant temperature and humidity box was built in order to grow crystals of the n-DA compounds by slow evaporation. Several crystals of 7-DA weighing about 5 mg were obtained. While these crystals are smaller than was hoped for and of a very poor quality, some information could still be obtained from them.

The Vibrating Sample Magnetometer

Most of the measurements which will be reported were obtained using a vibrating sample magnetometer. Since magnetization is also a function of applied field and temperature, our apparatus consists of several other subsystems in addition to the magnetometer itself. These include an electromagnet with field control, a cryostat with temperature measurement and control capability and a computer interfaced to these other systems.

The classic design of a vibrating sample magnetometer was developed by Foner.³⁸ Our magnetometer is however a commercial model, specifically an EG&G PAR model 155. A mechanical assembly vibrates a rigid sample rod at a frequency of 82.5 Hz (60 Hz and its harmonics are avoided because of power line noise). The sample in question is mounted at the lower end of the sample rod which is usually situated between the coils of a magnet. The lower portion of the rod is made of non-magnetic materials to

minimize background signals. As the sample vibrates it induces an ac current in pick-up coils mounted nearby. The ac signal from the sample has a frequency of 82.5 Hz and an amplitude proportional to the magnetization of the sample and to the amplitude of the vibration. Charged capacitor plates for which the air gap changes with the vibration provide a standard so that the detected signal can be made independent of vibrational amplitude. The signal then passes through a phase sensitive detector and the resultant magnetization is displayed in emu. The magnetometer is calibrated with a nickel standard for which the saturation magnetization per gram is well known.

The apparatus is equipped with a Janis Model 153 liquid helium cryostat made specifically for magnetometer measurements. Before a data collecting session the cryostat reservoir is filled with liquid helium. The helium is then metered through a needle valve and vaporized by a variable heater. The helium gas flows by the sample and the temperature of the sample is controlled by regulating the flow rate and the heater current. Temperatures from 300 K to 4 K can thus be achieved. By pumping on the sample chamber, the temperature of the helium gas can be reduced so that temperatures down to 1.7 K can be attained by this cryostat.

The temperature is monitored by carbon glass resistance thermometry. The carbon glass resistor is mounted on the sample rod as close to the sample as possible. A well controlled current is passed through the resistor and the voltage drop across the resistor is measured in order to determine its resistance, and then from a calibration chart the temperature is determined. Carbon glass is used for the sensor because of two important properties. The resistance changes are large at low temperatures making the thermometer sensitive to changes of less than one millikelvin at 4 K. Also, the resistance is very insensitive to the magnetic fields which must be applied to make magnetization measurements.

The magnetic field is generated by a Walker/Magnion laboratory electromagnet with a 3 1/2 inch pole gap. The magnet is powered by a Bridgewater, bipolar power supply which supplies currents of -25 to +25 amperes. In the magnet pole gap this corresponds to fields of -5500 to +5500 Oersted. The power supply is bipolar which means that the field can be swept continuously from positive to negative values without mechanical switching. This is important for low field measurements (below 50 Oe) and for obtaining hysteresis loops which need to be scanned through zero field. A Bell Model 160 Gaussmeter monitors the applied field.

The experiment can be computer controlled through an Apple IIE computer and an IEEE bus to a EG&G PAR model 145 VSM interface. The interface has two inputs which record the field being measured on the gaussmeter and the magnetization displayed on the magnetometer's panel meter. There is also one output for remotely controlling the applied magnetic field. As a future improvement to this apparatus, a direct IEEE line to a digital voltmeter is being considered so that temperature can also be recorded directly by the computer. Other hardware for data output from the computer includes a IEEE interfaced Houston Instruments DMP-40 Plotter and a parallel interfaced printer. All data are also stored on 5 1/4 inch floppy disks for archival purposes.

The software supplied with the magnetometer system is unfortunately not suitable for the type of measurements done in this laboratory. A set of routines has been written to allow one to utilize the time saving power of computer storage and retrieval. These programs are written in modules and include: A menu program for initiating other options; magnetometer operation programs for setting the magnetic field, collecting magnetization versus temperature and collecting magnetization versus field; output programs for printing data files and for plotting data and theoretical lines; and manipulation

programs for converting carbon glass resistance values to temperature, modifying data sets and fitting data to theoretical models.

All data fitting was done by computer using the simplex method.^{39,40} For n parameters an n -dimensional space is set-up. $(n + 1)$ guesses are made for a best fit, and these guesses form the corners of a simplex (a simplex being defined as a figure in an n -dimensional space having $n+1$ vertices). By calculating the standard deviation for these points, adjusting the simplex and recalculating repeatedly, the simplex moves and contracts until it converges on the best fit.

Measurements on CoNiTAC

Magnetization Versus Temperature Measurements

In addition to samples previously studied,²⁵ powder samples containing 50, 53, 58, 60 and 65 percent nickel were examined in order to determine their antiferromagnetic and spin glass transition temperatures. The powder susceptibility versus temperature curve for both zero field cooled and field cooled runs for the 53% sample is shown in Figure 6. At low temperatures the upper set of data represents the field cooled curve, and the lower set of data represents the zero field cooled curve. The temperature at which the curves join is the

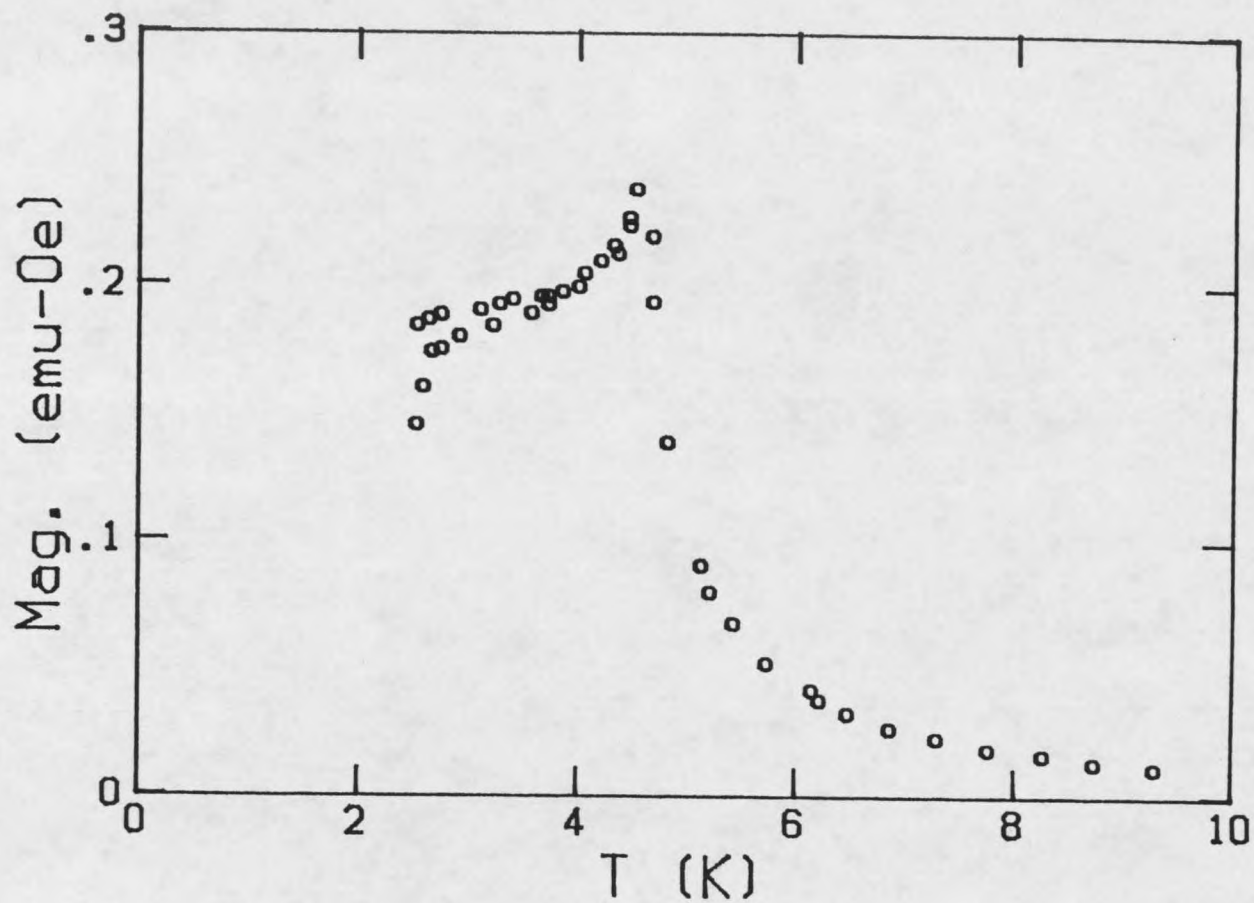


Figure 6. Magnetization versus temperature at 50 Oe for a powder sample containing 53% nickel. Both zero field cooled and field cooled curves are shown.

